Journal of Digital Imaging (2020) 33:1280–1291
https://doi.org/10.1007/s10278-020-00358-6

ORIGINAL PAPER

Simulating Tissues with 3D-Printed and Castable Materials

Michael O'Reilly[1] · Michael Hoff[1] · Seth D. Friedman[2] · James F. X. Jones[3] · Nathan M Cross[1]

Published online: 15 June 2020

Abstract

Manufacturing technologies continue to be developed and utilized in medical prototyping, simulations, and imaging phantom production. For radiologic image-guided simulation and instruction, models should ideally have similar imaging characteristics and physical properties to the tissues they replicate. Due to the proliferation of different printing technologies and materials, there is a diverse and broad range of approaches and materials to consider before embarking on a project. Although many printed materials' biomechanical parameters have been reported, no manufacturer includes medical imaging properties that are essential for realistic phantom production. We hypothesize that there are now ample materials available to create high-fidelity imaging anthropomorphic phantoms using 3D printing and casting of common commercially available materials. A material database of radiological, physical, manufacturing, and economic properties for 29 castable and 68 printable materials was generated from samples fabricated by the authors or obtained from the manufacturer and scanned with CT at multiple tube voltages. This is the largest study assessing multiple different parameters associated with 3D printing to date. These data are being made freely available on GitHub, thus affording medical simulation experts access to a database of relevant imaging characteristics of common printable and castable materials. Full data available at: https://github.com/nmcross/Material-Imaging-Characteristics.

Keywords 3D printing · Phantom · CT number · Hounsfield units · Medical simulation · Casting

Introduction

Additive manufacturing, rapid prototyping, or 3D printing, as it more commonly known, has exploded in popularity in recent years, although the underlying technology is not new. [1] Most frequently used in engineering disciplines, its use in medicine has coincided with the advent of relatively inexpensive commercial and retail 3D printers. Common uses in many hospitals include printing parts for education, fabricating medical imaging phantoms, and personalized treatment planning. [2–6] Publications in the medical literature have increased substantially compared to 10 years ago, demonstrating both the interest and applications for this manufacturing technology (Fig. 1).

3D printing encompasses a variety of different underlying technologies which all attempt to create a part by fusing material together layer by layer; thus, it is an additive manufacturing technique. Common commercially available technologies include extrusion-based fused deposition modeling (FDM), photopolymerization/stereolithography (SLA), binder jetting (BJ), and multijet fusion (MJF). For most of these technologies, both commercial and custom solutions exist. The most common printable materials in FDM printers (such as polylactic acid (PLA) are very rigid; however, there is a growing range of materials offering softer, more rubber-like properties using MJF and SLA technology. The softness/hardness of these materials is often expressed using the Shore Hardness Scale (0–100) of which there are 12 different standards. The two most commonly encountered standards are A and D, with the A being soft and D being hard. The Shore A scale is based on the induration caused by a 1.4-mm steel rod with a 0.79 mm diameter and 35° truncated cone applying 8.064 N of pressure. [7]

With the proliferation of different printing technologies, the wide range of available printable materials and their

Electronic supplementary material The online version of this article (https://doi.org/10.1007/s10278-020-00358-6) contains supplementary material, which is available to authorized users.

✉ Nathan M Cross
nathan.cross@gmail.com

[1] University of Washington, 1959 NE Pacific St., Seattle, WA, USA

[2] Seattle Children's Hospital, 4800 Sand Point Way NE, Seattle, WA, USA

[3] School of Medicine, University College Dublin, Dublin, Ireland

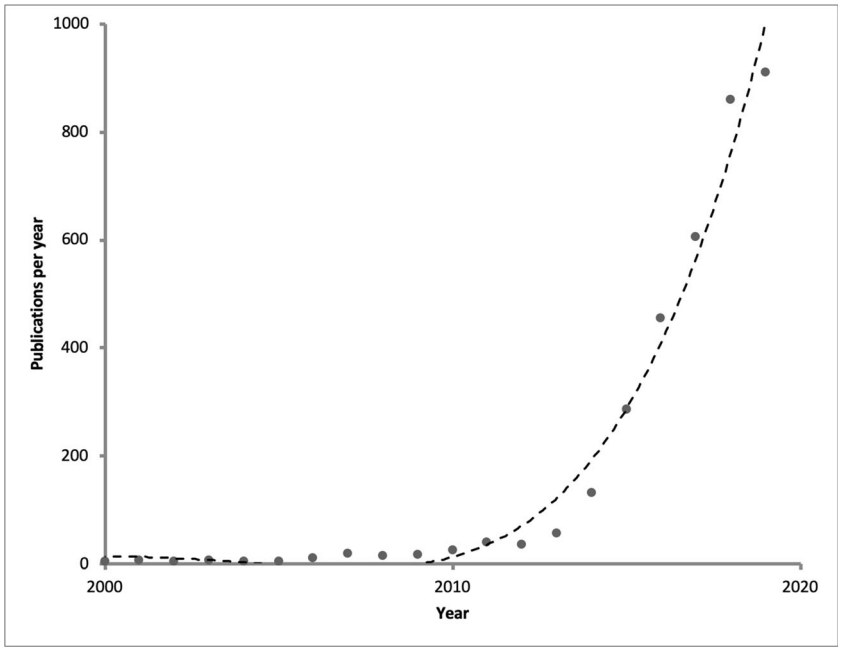

Fig. 1 Author's search of PubMed using search terms: ("3D Printing" OR "3-dimensional printing" OR "3D printed" OR "additive manufacturing" OR "rapid prototyping") AND ("Medicine") on November 7th 2019-PubMed maintained by the National Center for Biotechnology Information (NCBI), at the U.S. National Library of Medicine (NLM), located at the National Institutes of Health (NIH). Dashed line represents 5th order polynomial equation fitted to data ($R^2 = 0.98$)

characterization can be daunting in the early stages of planning a printing project. While most manufacturers list the specific physical properties of the materials such as Shore hardness or Youngs modulus, none list the expected linear attenuation coefficients that are intrinsic to the computation of CT number, measured with the Hounsfield Unit (HU) scale. This describes the linear attenuation coefficient of a material scaled by the attenuation values for water and air, where CT scanners are commonly calibrated such that water is approximately 0 HU and air is approximately − 1000 HU (Table 1). The particular HU value for a material is dependent on the material's atomic number (Z) and the CT kilovoltage (kV) setting chosen. This potential variability indicates why there are relatively few available resources that ascribe representative CT numbers to a broad range of 3D printed or castable materials. The largest record to date is by Bibb et al., who in 2011 listed 19 3D printing materials. [10] There have been 3 more recent publications with 14, 9, and 7 materials described using a variety of different printing technologies. [11–13] What are more common in the available literature are papers that describe a limited range of printable or bespoke materials evaluated by a range of cross-sectional imaging modalities often using differing scan parameters. [14–21] A review article by Filippou et al. is a nice synthesis of many of these papers and how these materials have been used in the 3D printing and radiology literature. [22]

Table 1 CT number in Hounsfield Units for materials in the ACR calibration phantom and common biologic tissues

Material	CT number range
Water	− 7 to + 7 HU[a]
Air	− 970 to − 1005 HU[a]
Acrylic	110 to 135 HU[a]
Polyethylene	− 107 to − 84 HU[a]
Teflon (bone)	850 to 970 HU[a]
Cortical bone	200 to 1000+ HU[b]
Medullary bone	50 to 200 HU[b]
Liver	50 to 70[b]
Blood	50 to 60[b]
Pancreas	30 to 50[b]
Kidney	20 to 40[b]
Fat	− 100 to − 80[b]
Lungs	− 950 to − 550[b]

[a] ACR CT Guidance Document [8]

[b] Principles of computed tomography, Willi Kalendar [9]

Although 3D printing can be used for virtually any manufacturing task, it must be emphasized that many tasks in model or phantom creation can also be achieved using castable material. Large volume models and casting techniques such as lost wax casting are both cheaper and easier to accomplish than 3D printing the same shape. Casting can also be a necessary adjunct to object creation if the material cannot be directly 3D printed.

The purpose of this paper is not to provide an overview of 3D printing itself, or an elaboration on the engineering properties of printable materials. Instead, we tackle a practical issue of clinical importance: what base materials should be selected to make a phantom that simulates different human tissues and yields realistic CT numbers? Based on practical experience, we hypothesize that there are custom and commercial solutions that can achieve accurate soft tissue and bone simulations not only in terms of structure and consistency but

also when imaged using CT. This paper aims to investigate many of the most commonly available commercial and retail 3D printing materials and some commonly used casting materials to aid the future design and manufacture of custom X-ray-based phantoms and procedural simulators.

Materials and Methods

Material Samples

A variety of samples were evaluated; some were fabricated by the authors and others were provided by the manufacturer (in total $n = 97$).

Custom Castable Materials

Common do-it-yourself (DIY) casting materials are shown in Table 2. Each material was poured into a 54 mm × 34 mm × 32 mm 3D-printed mold created on an Ultimaker FDM 3D printer (Ultimaker B.V. Burgemeester R., vd Venlaan, Geldermalsen, The Netherlands) to yield a 50 mm × 30 mm × 30 mm block (length × width × height).

All of these casting material blocks were fabricated using the manufacturer's instructions. All samples were degassed in a custom vacuum chamber at − 29 mmHg for 2 min to minimize bubble formation. The materials were cured at room temperature for 7 days prior to scanning.

Table 2 Consumer grade castable materials were cast by the authors into small blocks for scanning. Other materials in the master table were obtained in samples from the manufacturer

Manufacturer	Material
Middlesex University Teaching Rsrc Ltd.	Polymorph/Polycaprolactone
FullMoons Cauldron & Penreco	Gel Wax
Smooth-On Inc.	Body Double 25A
Smooth-On Inc.	Dragon Skin 10A
Smooth-On Inc.	Dragon Skin 20A
Smooth-On Inc.	Dragon Skin FX Pro
Smooth-On Inc.	DragonSkin
Smooth-On Inc.	Eco Flex 00–30
Smooth-On Inc.	Eco Flex 00–30 10% thin
Smooth-On Inc.	Eco Flex 00–30 5% thin
Smooth-On Inc.	Eco Flex 00–50
Smooth-On Inc.	Feather Light Resin
Smooth-On Inc.	Mold Max 10A
Smooth-On Inc.	Mold Max 20A
Smooth-On Inc.	Mold Max 40A
Smooth-On Inc.	Solaris 15A

Manufacturer-Supplied Samples

Several manufacturers of castable materials not commonly available to the hobbyist or entry-level consumer (including Axson-Technologies, and HEI-Cast.) provided samples of castable materials. These materials came in a variety of shapes and sizes, but all were of a sufficient size to image (Fig. 2).

Commercial 3D-printed samples were obtained from a digital manufacturing service (Fathom, 620 3rd Street Oakland, CA, USA); these included HP multi-jet fusion, extensive variations of binder-jetting materials, and the full range of Stratatsys elastomers and DM400, one of a new class of "biomimicry" options.

3D Printing

An initial set of different 3D-printed blocks were made from commonly available materials on several different types of printer. Solid binder jet 3D-printed 1.5-cm^3 blocks were manufactured on a ZPrinter 250 3D printer (3D Systems Corp., Rock Hill, SC) using ZP151 powder with additional blocks post processed using ZBond and Epsom salts. An Ultimaker Original FDM 3D printer using Ultimaker Orange 2.8 mm PLA was used to create 25%, 50%, and 100% infill blocks and Ultimaker 2.8 mm ABS to create a 100% infill block. An Objet Eden 250 (Stratasys, 7665 Commerce Way Eden Prairie, MN 55344 United States) using Objet VeroWhite was also used to make an SLA block.

Further sets of 3D-printed blocks were assembled at later dates, printed in house on a variety of printers. Several FDM blocks were created on a modified Lulzbot Taz 5 (Aleph Objects, Inc. Loveland, CO, USA) with varying degress of infill (30%, 45%, 60%, 75%, 90%, and 100%) in High Impact Polystyrene (HIPS) and an optimized form of polylactic acid

Fig. 2 Multiple samples were assembled on Siemens Somatom Definition AS+ scanner with an ACR phantom used for scanner calibration. The scans were repeated for multiple kVs and ROIs were measured to determine the CT number of each sample

(PLA): PLA Pro (Shenzhen eSun Industrial Co Ltd., Shenzhen, China) (Fig. 3). A set of SLA print blocks were made on a Form 2 printer (Formlabs Inc., 35 Medford St. Suite 201 Somerville, MA 02143 USA) using Black v2, Clear v4, White v1, Durable v2, Flexible v2, High Temp v1, Tough v5, and Dental v1 resins. An additional Z Corporation Z250 powder printer was used to print several samples and one was postprocessed by soaking it in cyanoacrylate (similar to the propriatry Zbond) to harden the material, a common method to increase the durability and hardness of these prints.

ACR Phantom

The CT American College of Radiology (ACR) 464 phantom (Gammex, A Sun Nuclear Company, 7600 Discovery Drive, Middleton, WI 53562) was employed to provide reference CT numbers for a few standard materials. This phantom is normally employed to assess imaging performance and compliance with ACR standards and regulations [12] on a routine basis in clinical practice. Module 1 of the phantom allows assessment of CT number accuracy. It includes standardized inserts that mimic the exact attenuation characteristics of polyethylene, water, acrylic, bone, and air and may thus be used as a reference for further measurements of attenuation via CT number [12].

Computed Tomography Imaging

CT Protocol

Similar scanning protocols were employed at the two research sites: Mater Misericordiae University Hospital in Dublin, Ireland (MMUH), and the University of Washington Harborview Medical Center (UW-HMC). CT scanning at both sites was performed using Siemens SOMATOM Definition AS+ 128 slice scanners (Siemens Healthineers; Erlangen, Germany). Variable sets of commercially-sourced and 3D-printed material blocks were assessed at each site, with some materials scanned at both sites (e.g., ABS) to provide an internal standard/control. All material samples were aligned with the scanner bed and the bore axis to minimize partial volume effect during measurements. Scans employed a detector configuration of 128 × 0.6 mm (flying focal spot, nominal radiation beam width of 38.4 mm) to execute a standard spiral head CT protocol technique with automated tube current modulation to yield axial images reconstructed using a J30s medium smooth kernel at a display field of view of 27.6 cm. Coronal reconstructions were generated from these axial acquisitions.

There were some subtle CT protocol deviations between the two sites. At MMUH, a 120 kV scan with a 0.55 pitch factor and an effective mAs of 291 was employed. At the UW-HMC, images were acquired at 80, 100, 120, and 140 kV, with 0.50 pitch factor and an effective mAs of 250.

CT Analysis

Data in the Digital Imaging and Communications in Medicine (DICOM) format was exported from each CT scanner and imported into a free open source medical image viewer, Horos (https://horosproject.org, Nimble Co LLC, Annapolis, MD USA). Slice data was reviewed

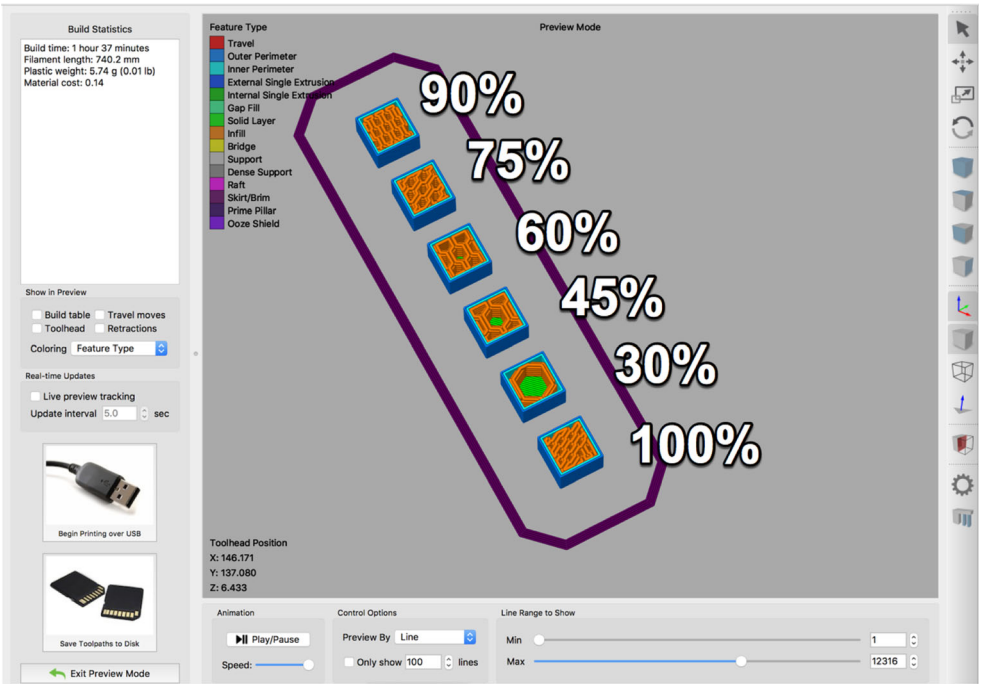

Fig. 3 Path analysis tool of Simplify3D demonstrating planned infill of a set of sample cubes to be printed on a modified Lulzbot Taz 5. Color corresponds to the purpose of the material to the part. Percentage of infill is labeled next to each sample

in axial and coronal reconstructions depending on the alignment of the sample piece. As mentioned in the sample section, there was significant variability in size and shape of the samples depending on the source of the sample. Some manufacturer samples were of materials not readily available on the market and thus more convenient shapes could not be made or obtained. Regions of interest (ROI) were positioned over each material in 5-mm-thick reconstructed slices. The closest plane to parallel with the longest axis of the sample that passed through the center of each sample was selected for measurement. This maximized the area of material in the plane of reconstruction. The area of the rectangular measurement ROI was maximized to include as much material as possible, without getting too close to the edge of the block and maintaining a 2–3 pixel distance from the edge of the sample, similar to the methodology of Bibb et al. [10] This was done to minimize artifacts and partial volume effects with air at the boundary of the sample (Fig. 4). This resulted in variable sizing of ROIs but the largest sampling of material to maximize the number of voxels sampled and improve reported CT number accuracy.

The material's CT number was computed from the material's attenuation coefficient, scaled relative to a CT number for air of −1000 HU and water of 0 HU. Since the attenuation coefficients of substances other than water are energy-dependent, most materials were scanned at several tube voltages (80 kV, 100 kV, 120 kV, 140 kV) to characterize their HU across a variety of x-ray energies. The average CT number and its standard deviation were reported for each of the scans at each kV.

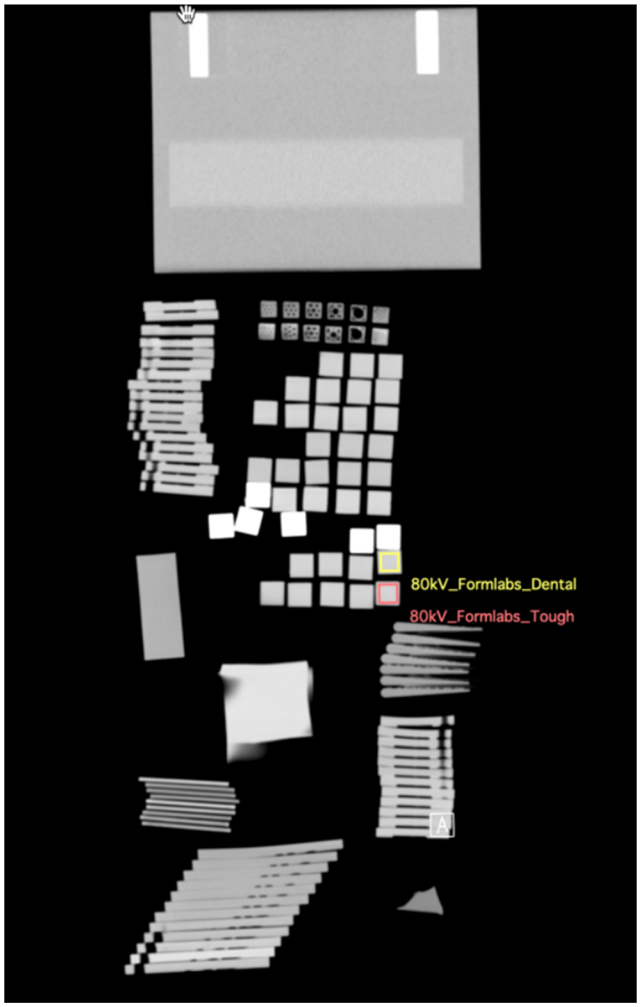

Fig. 4 An example image slice of one of the scans through the material set. DICOM files from the scans were loaded into a DICOM image viewer-Horos and were reviewed in the axial or coronal plane. ROIs were placed over each block on the axis aligned with the longest axis of the sample to maximize the area of the ROI relative to the sample and to minimize any artifact included within the ROI

Costs

Comparing material costs can be challenging given that some printing processes are not solid, and many materials are sold in volumetric versus weight-based units. For example, FDM materials are usually sold in spools of filament and priced per kilogram of material. On the other hand, resins for stereolithography are often priced per liter of resin. This complication was obviated in this study by using density information from the manufacturer to help calculate the price per unit volume for each material in USD. Additionally, with FDM, there is a solid outer shell and usually an internal lattice that is only partially solid. As an approximation, 5% was added to the infill value to account for the solid shell of the part and the result was multiplied by the price for the raw material. This reduction in cost was estimated for the non-solid FDM materials (eSUN HIPS and PLA).

The pricing was obtained from large commonly available US online retailers for small quantity orders (a spool of filament, a single 1 L unit of resin). An additional qualitative assessment of material price was created to summarize these findings.

Ancillary Data

To help readers understand the variety of materials and their potential uses, some additional data describing the manufacturing process used to form the sample was reported. This included casting: vacuum cast, slush cast; and 3D printing processes: FDM, BJ, SLA, selective laser sintering (SLS), and MJF. These processes are all available to the user through online manufacturing services, and some are readily achievable in a small lab or hobby setting. To facilitate research, the datasheet links are also provided.

Results

CT Number

The average CT number and standard deviation were recorded for all 102 materials scanned (also including the five materials in the ACR phantom). Materials in the second set of scans had measurements at multiple tube kilovoltages, which can be seen in the supplementary materials. The average CT number of the different materials varied from − 992 to 1458 HU. Many of the 3D-printed plastics/resins (SLA and FDM) exhibited CT numbers from − 150 to + 150 HU.

Large standard deviations are seen with all the Esun PLA and HIPS prints due to the varied infills used for the samples. These samples are subsolid and the structure of the infill is at a larger scale than the dimensions of the voxels; thus, an ROI of the HIPS samples with different infills contains a variable percentage of voxels of air vs plastic (HIPS). This results in a partial volume effect: some voxels have a CT number closer to the plastic, and others have the CT number closer to air, creating a large CT number standard deviation as the variable plastic/air proportion results in a varying average HU value. See Figs. 3 and 5 to see the proportion of infill for each of the samples.

Metadata

The table of materials encompasses a wide variety of the materials that are worked with using different manufacturing techniques and lists additional metadata such as manufacturer information. The Shore hardness was included for all materials, apart from gel wax, for which the authors' estimate is provided. A description of the color of the material was reported, as well as the underlying type of plastic or resin. An additional column summarizes the type of 3D printing process or casting process used to work with the material. Links to manufacturers' data sheets are also provided where available.

Cost

Materials were classified by price, summarized in Table 3. In general, the SLA resins for Formlabs printers are around $150–200/L and other SLA printers' resins may cost more. FDM is more affordable in general with spools of filament costing around $25–50/L (but usually being sold as a spool of filament weighing 1 kg).

Powder-based printing materials are slightly less expensive than SLA materials at around $115/L.

Of the castable materials, Gel wax is one of the cheapest materials on the list at about $8–16/L depending on the manufacturer. Many castable materials, mostly silicone, are either similar in price or range up to twice that price.

To facilitate the ready availability of this table of materials, it has been listed publicly on GitHub (https://github.com, Github Inc., 88 Colin P Kelly Jr St, San Francisco, CA 94107). GitHub is a service frequently used for dissemination and versioning of programming code but affords an accessible location where this database of materials can be freely and easily accessed, and anyone can extend the catalog or make revisions as needed. The authors will update as data becomes available within their lab. The complete table can be found in XLSX and comma separated value format at the following address: https://github.com/nmcross/Material-Imaging-Characteristics, and excerpts are present in the supplementary materials.

Discussion

Expanding interest in 3D printing has resulted in the development of many new printing materials with their own unique physical properties. Although 3D printing has been used in imaging phantom production, it is often unclear how the materials were selected, whether by trial and error, or simply according to material availability. This is the largest study to date assessing multiple different parameters associated with 3D printing and casting materials.

CT Number and Physical Properties

Table 1 shows that the human body encompasses a wide range of CT numbers [HU], from dense bone with a HU of over 1000 to the aerated lungs at − 950. Most soft tissues lie in the range of 15–90 HU, excluding fat/adipose tissue at approximately − 80 to − 100 HU. [23] While many of the materials we scanned lie at the extremes of biologic tissue CT numbers, similar to previous studies, some would be useful in creating CT phantoms or procedural simulators. [10, 11, 13, 21] Additionally, for simulators, one needs to take the physical properties of the printed or castable material into consideration. We attempted to provide this information in terms of the Shore scale, a standardized method of measuring the softness/firmness of materials. We did not make these measurements ourselves, and the values quoted were extracted, when available, from the material properties sheets supplied by the manufacturer. In Table 4, we list examples of materials that we feel have similar radiological and physical properties to real tissues. However, these are based on clinical experience through procedural work and are not statements regarding the actual physical properties of the tissues listed. We are not aware of any published literature that has reliably measured the Shore hardness of different human tissues.

ZPrinter 151 gypsum powder is a material ideally suited for printing bone-like structures, with CT numbers ranging from 500 to 1000 HU, depending on the use of different post-

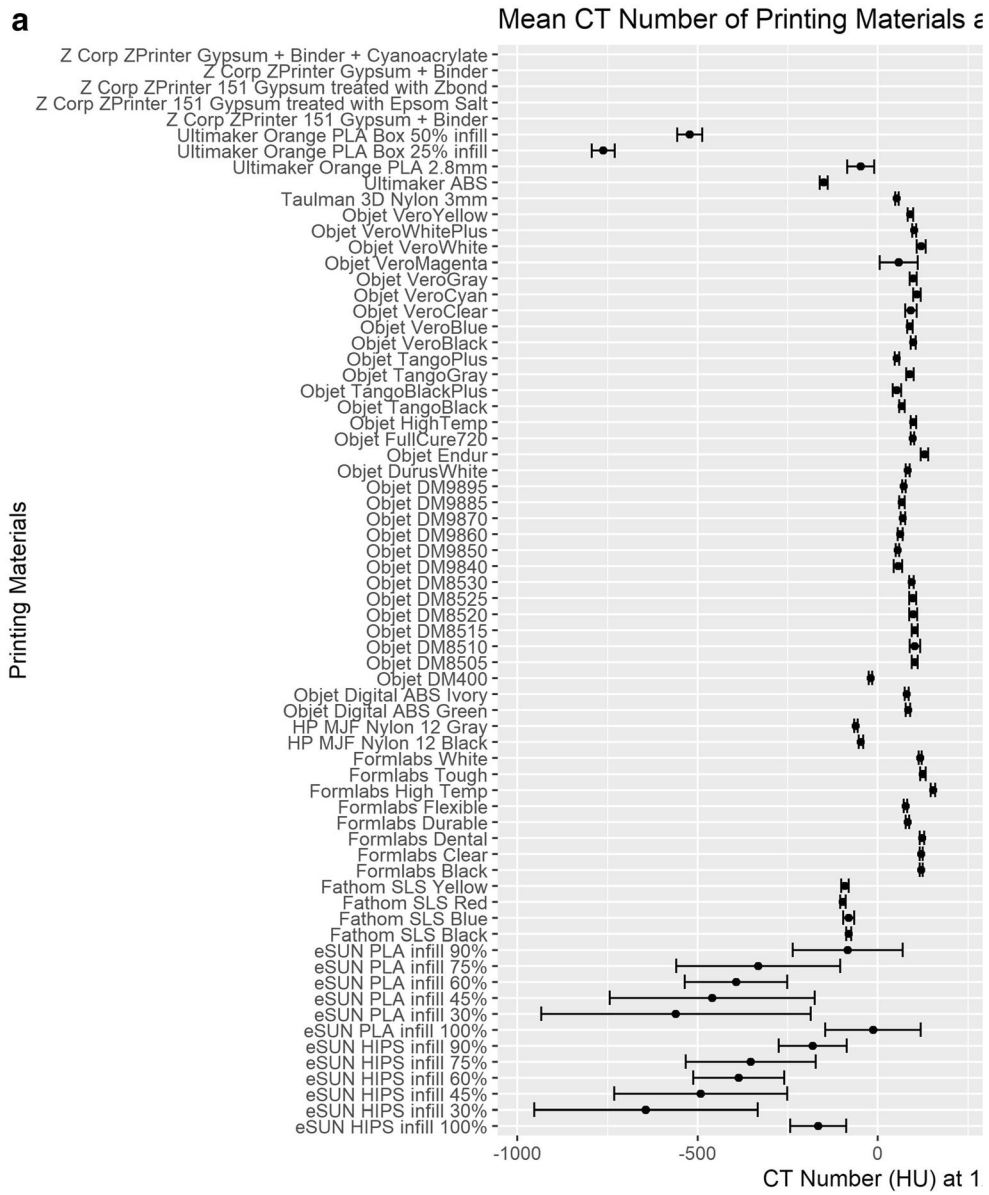

Fig. 5 **a** Comparison of multiple printing materials measured CT number in Hounsfield units (HU). The large standard deviation noted in the eSun materials is because they were printed using FDM and are not solid, thus an ROI over this material includes both air and plastic. There was a notable variation in measured CT number for the materials that were quite dense. **b** Comparison of multiple casting materials measured Hounsfield units (HU)

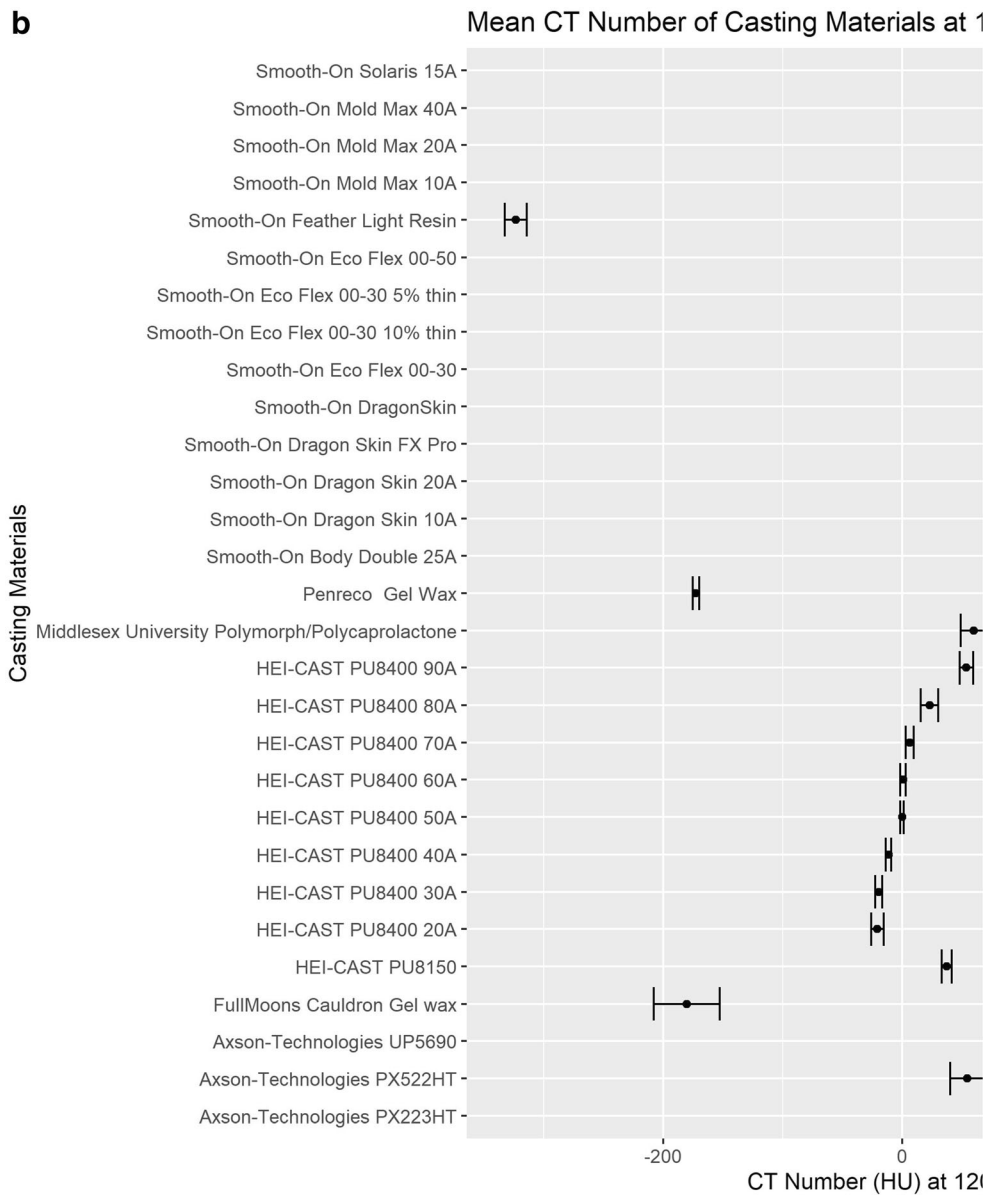

Fig. 5 (continued)

processing materials such as cyanoacrylate similar to previous investigation. [10] BJ printers such as a ZP 250 (3D Systems Corp., Rock Hill, SC) can simulate the different components of bone via its manufacturing process; the harder outer cortex and medullary striations are fused using binder and internal softer, less dense medullary bone is left unbound during printing to yield a lower CT number from segmented CT scans. Figure 6 is an example of the cranial vault and cervical spine produced by the authors using a ZP250 printer.

Many of the Objet SLA printable materials had CT numbers in the expected range of soft tissue within the body. TangoBlack Plus had a CT number of 52.1 HU when scanned at 120 kV and was relatively soft with a Shore hardness of 26–28 A. This material could be used to emulate liver or other soft tissue organs. The softness of the material could be exploited to create a phantom that would allow trainee doctors to practice biopsies or treatments such as tumor ablation with more realistic haptic feedback. In addition, given that many Objet printers are multimaterial printers, a liver with a tumor of differing radiodensity and color to improve the fidelity and realism of CT-based procedural simulations can be printed. TangoBlack Plus has been evaluated by CT in a previous study; however, the actual measured CT number was not reported. [12] Other imaging characteristics associated with MRI or Ultrasound were outside the scope of this study but are of future interest to the authors. There is a known difficulty in finding materials that behave as their biological counterpart across imaging modalities. [22]

Table 3 A portion of the table showing relative pricing of various materials. Some materials have been removed because they are repetitive but can be reviewed in the full version of the table online

Source	Material description	Manufacturing process as tested	Approximate material price ($USD/L)
Formlabs Inc.	Black	SLA	$149
Formlabs Inc.	Clear	SLA	$149
Formlabs Inc.	Dental	SLA	$149
Formlabs Inc.	Durable	SLA	$175
Formlabs Inc.	Flexible	SLA	$199
Formlabs Inc.	High Temp	SLA	$199
Formlabs Inc.	Tough	SLA	$175
Formlabs Inc.	White	SLA	$149
FullMoons Cauldron	Gel wax	SC	$9
Middlesex University	Polymorph/Polycaprolactone	SC	$33
Objet	Digital ABS Green	SLA	$300
Objet	Digital ABS Ivory	SLA	$300
Objet	DM400	SLA	$300
Objet	DurusWhite	SLA	$300
Objet	Endur	SLA	$300
Objet	FullCure720	SLA	$300
Objet	HighTemp	SLA	$300
Objet	TangoBlack	SLA	$300
Objet	TangoBlackPlus	SLA	$300
Objet	TangoGray	SLA	$300
Objet	TangoPlus	SLA	$300
Objet	VeroBlack	SLA	$300
Objet	VeroBlue	SLA	$300
Objet	VeroClear	SLA	$300
Objet	VeroCyan	SLA	$300
Objet	VeroGray	SLA	$300
Objet	VeroMagenta	SLA	$300
Objet	VeroWhite	SLA	$300
Objet	VeroWhitePlus	SLA	$300
Objet	VeroYellow	SLA	$300
Penreco	Gel Wax	SC	$17
eSUN	HIPS infill 100%	FDM	$24
eSUN	PLA infill 100%	FDM	$30
Smooth-On	Body Double 25A	VC	$49
Smooth-On	Dragon Skin 10A	VC	$38
Smooth-On	Dragon Skin 20A	VC	$38
Smooth-On	Dragon Skin FX Pro	VC	$39
Smooth-On	DragonSkin	VC	$38
Smooth-On	Eco Flex 00–30	VC	$38
Smooth-On	Eco Flex 00–30 10% thin	VC	$34
Smooth-On	Eco Flex 00–30 5% thin	VC	$36
Smooth-On	Eco Flex 00–50	VC	$38
Smooth-On	Feather Light Resin	VC	$16
Smooth-On	Mold Max 10A	VC	$33
Smooth-On	Mold Max 20A	VC	$32
Smooth-On	Mold Max 40A	VC	$29
Smooth-On	Solaris 15A	VC	$56
Taulman 3D	Nylon 3 mm	FDM	$45
Ultimaker	ABS	FDM	$26
Ultimaker	Orange PLA 2.8 mm	FDM	$29
Ultimaker	Orange PLA Box 25% infill	FDM	$9
Ultimaker	Orange PLA Box 50% infill	FDM	$16
Z Corp	ZPrinter 151 Gypsum + Binder	BJ	$112

VC vacuum cast, *FDM* fused deposition modeling, *SLA* stereolithography, *SLS* selective laser sintering, *BJ* binder jetting, *SC* slush cast

Although there is much interest in the use of 3D printing to produce imaging and simulation phantoms in medicine, some tasks can be more easily achieved with older casting techniques. Many of these casting materials have not been evaluated before. This justifies their inclusion in the present study and it is important to recognize that they can be cheaper and less time-consuming alternatives to 3D printing. Models that could be difficult and costly to achieve with 3D printing, such as filling voids in the abdomen or the cranial vault, are easier to produce using older manufacturing methods. [12] Gel wax

Table 4 Materials scanned that may be suitable as physical and radiological biologic mimics. The shore hardness stated relates only to the 3D printed or castable material, and the authors' opinion as to what biological tissue this is suitable to mimic

Material	Technology	Shore hardness	Tissue mimic	Observed CT number	Expected CT number
Zprinter Gypsum	3D-BJ	75D	Cortical Bone	528–935	200–1000
DM9840	3D-SLA	35–40 A	Liver	41–60	50–70
TangoBlack(plus)	3D-SLA	26–28 A	Kidney	21–51	20–40
Gel Wax	Casting	< 60 00	Fat	36	20
Dragon Skin 10A	Casting	10 A	Medullary Bone	156–261	50–200

is an ideal material when one needs to recreate fat, as it has a similar HU range and physical properties to adipose tissue. [24]

Costs

When embarking on a project or study involving 3D printing of true scaled anatomy, costs can quickly escalate given the amount of substrate/material that may be required. In the full table of results available in the supplementary materials or online at https://github.com/nmcross/Material-Imaging-Characteristics, we have categorized each printable material according to expense and also the fabrication service needed from the hobbyist to the professional level. FDM materials are usually the cheapest 3D printing materials, but their CT number can be less suited to phantom production (apart from the lungs or other aerated structures) and the easier to print materials are usually rigid and brittle. Powder-based printing materials are slightly less expensive than SLA materials at around $115/L but produce prints with very different material characteristics to plastics. Multi-jet fusion and laser sintering are less common processes on higher end machines and most commonly available through commercial vendors on a fee-per-print basis. Gel wax is one of the cheapest materials on the list at about $8–16/L, depending on the manufacturer. Other castable materials such as silicones are twice as expensive as gel wax but similar in price to FDM materials.

Often, procedural simulators are destroyed in the process of using them and some relatively simple commercially produced simulators can cost thousands of dollars. 3D printing can be used to create relatively inexpensive simulators or replace consumable parts in existing simulators. [13, 25]

In this study, we did not assess the cost of the printer itself, which can be substantial. SLA and particularly FDM have some inexpensive printers which are widely available at the consumer level. While this may be thought of as a single capital expense, the less expensive systems may have substantial maintenance and tuning costs associated, particularly in man-hours required to keep these systems operational. While this component of printer ownership is becoming more manageable with improved designs and software, variation in FDM material characteristics between different colored plastics or the same plastic from different vendors can subtly change the melt point or print characteristics, requiring a slow tuning process to discover optimal print settings. Different print processes and the maintenance associated with them should be carefully investigated prior to investing in a printer.

A wide variety of commercial printing services are available online (such as Shapeways.com, 3dhubs.com,

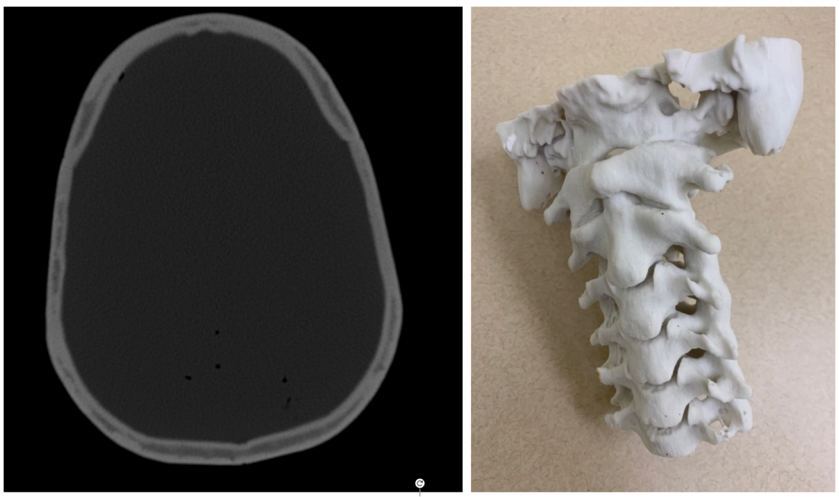

Fig. 6 CT scan of a 3D-printed cranial vault and photograph of a cervical spine print using a ZP250 printer and ZP151 powder

craftcloud3d.com) which make it easy to see the kinds of results one can obtain from different printing processes without investing in a printer.

Limitations

The limitations of this study include the large standard deviation in CT number observed in some materials due to their inhomogeneity and in some cases the binders used. This has previously been documented for scenarios using the same material from different vendors. [11] In the case of the Z250 printer, cyanoacrylate or glue used to strengthen some models only penetrates the material by a few millimeters. As a result, the measurements were affected by the proportion of the ROI containing glue-hardened powder versus powder and printed binder. Non-linearities in HU as a function of kV were expected and observed in some materials, particularly when their Z numbers were quite different from that of water or air. In practice, differences in measured CT number when changing kV can be exploited for tissue characterization in medicine using applications such as dual-energy CT scanning.

While this is the largest collection of materials cataloged to date, only a fraction of materials available are listed, and the study does not represent all 3D printing technologies or materials. There are a multitude of different manufacturers of 3D printing materials, and the exact compositions of the materials may be variable, proprietary, or unavailable. The focus was to characterize these materials for usage in CT, radiographic or fluoroscopy phantoms and understand their imaging appearance relative to human tissues. The materials of the present study were selected for a variety of reasons including ease of use, ready availability, tissue-mimicking imaging characteristics, and cost.

Because of the large number of samples obtained and material availability from different manufacturers, there was variation in the size and shape of the materials, as can be seen in Figs. 2 and 4. However, as the scans were performed at a resolution of 0.625 mm, there was an adequate sample of voxels to estimate the CT number, and repeated measurements were made as the table was being constructed to ensure reproducibility. Measurements were made on scanner systems at two institutions to increase the number of samples, and while the scanning parameters used were nearly identical, there were slight variations due to software and model differences. Other vendors and models were not tested to determine the effects of scanner variability on CT number. The materials were scanned in air, which may create some boundary artifacts at the air material interface. The edge of regions of interest were carefully placed a few voxels away from the boundary to minimize artifactual effects on the measured values.

Cost estimations were based on small volume usage of materials purchased in the United States of America. Availability in other countries and pricing, shipping, or handling could be different in other countries. Also, if models are being manufactured routinely in a lab, there may be more economical ways of purchasing materials, or third-party resins which could reduce cost.

Although there have been some ingenious recent methods for directly controlling radiodensity during the printing process itself (through bismuth infusion of ABS filaments, iodine impregnation of paper), the present study has focused exclusively on off-the-shelf manufacturing processes and materials. [26, 27]

Case Example

Since completing this study, we have utilized our own database to plan, develop, and prototype a novel clinical simulator for C1/2 cervical cerebrospinal fluid (CSF) punctures, which are often performed by neuroradiologists using X-ray or CT guidance. These procedures occur when it is not possible to sample CSF via the traditional lumbar technique. [28] These are rare procedures, and so teaching of this technique is often sporadic and haphazard. Creating a realistic and reusable simulator could improve confidence and allow a medical doctor to practice in advance. The constituents of the model comprise the bone of the cervical spine, soft tissues of the neck, CSF and the spinal cord. Using our database we selected Zprinter gypsum, gel wax, water and TangoBlack(plus) respectively to mimic these tissues. The cervical spine for the model can be seen in Fig. 6. This bespoke simulator can be conceived and used to fill gaps in clinical education but represents a type of model generation that is likely too specialized to be commercially viable for a company to undertake.

Conclusions

The manufacture of high-fidelity imaging anthropomorphic phantoms and simulators requires precise three-dimensional material distribution of a reliable radiopacity, with the ability to alter physical properties as appropriate. No commercially available 3D printers can do this yet. This library is the first step in cataloging the multi-voltage CT attenuation characteristics and physical properties of currently available 3D printed and castable materials. Future progress in 3D printing technology may supplement the collection to better replicate the spectrum of radiodensity found in the human body.

Acknowledgments Christopher Howard, Seattle Children's Imagination Lab–multiple print samples.
David Zamora MS, UW Radiology–help with CT Physics.
Christina Brunquell PhD, UW Radiology–help with CT Physics.
Kalpana Kanal PhD, UW Radiology–help with CT Physics.

Compliance with Ethical Standards

Conflict of Interest The authors declare that they have no conflict of interest.

References

1. Hull CW. Apparatus for production of three-dimensional objects by stereolithography. Google Patents; 1986.
2. Dong M, Chen G, Li J, Qin K, Ding X, Peng C, et al. Three-dimensional brain arteriovenous malformation models for clinical use and resident training. Medicine (Baltimore) 2018;97(3):e9516.
3. Hernandez-Giron I, den Harder JM, Streekstra GJ, Geleijns J, Veldkamp WJH. Development of a 3D printed anthropomorphic lung phantom for image quality assessment in CT. Phys Med 2019;57:47-57.
4. Mao Z, Zhang N, Cui Y. Three-dimensional printing of surgical guides for mandibular distraction osteogenesis in infancy. Medicine (Baltimore) 2019;98(10):e14754.
5. Shibata E, Takao H, Amemiya S, Ohtomo K. 3D-printed visceral aneurysm models based on CT data for simulations of endovascular embolization: evaluation of size and shape accuracy. AJR Am J Roentgenol 2017;209(2):243-7.
6. Wong TT, Lynch TS, Popkin CA, Kazam JK. Preoperative use of a 3D printed model for femoroacetabular impingement surgery and its effect on planned osteoplasty. Am J Roentgenol 2018;211(2): W116-W21.
7. Mix A, Giacomin A. Standardized polymer durometry. J Test Eval 2011;39(4):696-705.
8. Dillon C BW, Clements J, Cody D, Gress D, Kanal K, Kofler J, McNitt-Gray MF, Norweck J, Pfeiffer D, Ruckdeschel TG, Strauss KJ, Tomlinson J. Computed tomography quality control manual. . Reston:American College of Radiology; 2017.
9. Kalender W. Computed tomography: fundamentals, system technology, image quality, applications. 2011. Translated from the German.
10. Bibb R, Thompson D, Winder J. Computed tomography characterisation of additive manufacturing materials. Med Eng Phys. 2011;33(5):590-6.
11. Shin J, Sandhu RS, Shih G. Imaging properties of 3D printed materials: multi-energy CT of filament polymers. J Digit Imaging 2017;30(5):572-5.
12. Silvestro E, Betts KN, Francavilla ML, Andronikou S, Sze RW. Imaging properties of additive manufactured (3D printed) materials for potential use for phantom models. J Digit Imaging 2019
13. Mooney JJ, Sarwani N, Coleman ML, Fotos JS. Evaluation of three-dimensional printed materials for simulation by computed tomography and ultrasound imaging. Simul Healthc 2017;12(3): 182-8.
14. Matsumoto JS, Morris JM, Foley TA, Williamson EE, Leng S, McGee KP, et al. Three-dimensional physical modeling: applications and experience at Mayo Clinic. Radiographics 2015;35(7): 1989-2006.
15. Hazelaar C, van Eijnatten M, Dahele M, Wolff J, Forouzanfar T, Slotman B, et al. Using 3D printing techniques to create an anthropomorphic thorax phantom for medical imaging purposes. Med Phys 2018;45(1):92-100.
16. Adams F, Qiu T, Mark A, Fritz B, Kramer L, Schlager D, et al. Soft 3D-printed phantom of the human kidney with collecting system. Ann Biomed Eng 2017;45(4):963-72.
17. Jahnke P, Limberg FR, Gerbl A, Ardila Pardo GL, Braun VP, Hamm B, et al. Radiopaque three-dimensional printing: a method to create realistic CT phantoms. Radiology. 2017;282(2):569-75.
18. Okkalidis N, Marinakis G. Technical note: accurate replication of soft and bone tissues with 3D printing. Med Phys. 2020:https://doi.org/10.1002/mp.14100.
19. Imstorfer N, Unger E, Hojreh A, Homolka P. An anthropomorphic phantom representing a prematurely born neonate for digital x-ray imaging using 3D printing: proof of concept and comparison of image quality from different systems. Sci Rep. 2019;9(1):14357.
20. Javan R, Cho AL. An assembled prototype multimaterial three-dimensional–printed model of the neck for computed tomography–and ultrasound-guided interventional procedures. J Comput Assist Tomogr 2017;41(6):941-8.
21. Dancewicz OL, Sylvander SR, Markwell TS, Crowe SB, Trapp JV. Radiological properties of 3D printed materials in kilovoltage and megavoltage photon beams. Phys Med 2017;38:111-8.
22. Filippou V, Tsoumpas C. Recent advances on the development of phantoms using 3D printing for imaging with CT, MRI, PET, SPECT, and ultrasound. Med Phys 2018;45(9):e740-e60.
23. Kalender WA. Computed tomography: fundamentals, system technology, image quality, applications John Wiley & Sons; 2011.
24. Vieira SL, Pavan TZ, Junior JE, Carneiro AA. Paraffin-gel tissue-mimicking material for ultrasound-guided needle biopsy phantom. Ultrasound Med Biol 2013;39(12):2477-84.
25. Chang D, Tummala S, Sotero D, Tong E, Mustafa L, Mustafa M, et al. Three-dimensional printing for procedure rehearsal/simulation/planning in interventional radiology. Tech Vasc Interv Radiol 2019;22(1):14-20.
26. Ceh J, Youd T, Mastrovich Z, Peterson C, Khan S, Sasser TA, et al. Bismuth infusion of ABS enables additive manufacturing of complex radiological phantoms and shielding equipment. Sensors (Basel). 2017;17(3).
27. Jahnke P, Schwarz S, Ziegert M, Schwarz FB, Hamm B, Scheel M. Paper-based 3D printing of anthropomorphic CT phantoms: feasibility of two construction techniques. Eur Radiol 2019;29(3):1384-90.
28. Daniels SP, Schweitzer AD, Baidya R, Krol G, Schneider R, Lis E, et al. The lateral C1-C2 puncture: indications, technique, and potential complications. Am J Roentgenol 2019;212(2):431-42.